A study of the applicability of the renormalization group idea to multichain lattice systems by numerical experiments

Hiroshi Okamoto

Citation: The Journal of Chemical Physics **88**, 5095 (1988); doi: 10.1063/1.454663
View online: http://dx.doi.org/10.1063/1.454663
View Table of Contents: http://scitation.aip.org/content/aip/journal/jcp/88/8?ver=pdfcov
Published by the AIP Publishing

A study of the applicability of the renormalization group idea to multichain lattice systems by numerical experiments

Hiroshi Okamoto
Department of Systems Engineerings, Nagoya Institute of Technology, Gokisomachi Shouwaku, Nagoya, 466, Japan

(Received 21 July 1986; accepted 16 December 1987)

Our numerical experiments aim to study the applicability of the renormalization group (RG) idea to multichain lattice systems. The systems are composed of multiple chains on a simple cubic lattice. The nearest-neighbor interaction is assumed between nonbonded chain elements. The RG parameter space is spanned by the inverse of the chain length $1/n$, the solvent condition η, and the chain number concentration ρ. We first tentatively determine parameter flows by using two RG invariants (weak conditions). Then we examine whether the flows satisfy the RG requirements for the correlations (strong conditions). Simultaneous satisfaction will guarantee us the applicability of the RG idea. We found that the RG idea is applicable to the systems in the very good solvent region but becomes inapplicable to those in the poorer solvent regions and to the shorter spatial distances. In the range where the linearized RG defined by a fixed point in the good solvent region works successfully, we arrive at scaling forms in several fashions. One of them corresponds to Freed's crossover form. The RG appears to work even in the nonlinear range, i.e., concentrated solutions outside the semidilute region. The RG failure in the poor solvent region is briefly discussed.

I. INTRODUCTION

The renormalization group (RG) has been utilized as a tool constructing the universal relations in long chain solutions. The universality concept was first motivated by an analogy between zero-dimensional spin systems under a magnetic field and long chain solutions.[1] Later, the concept was studied by the RG along a chain such as in the blob theory[1] and the conformational space RG (CSRG) theory.[2,3]

The universality asserts that the properties of long chain solutions, such as the reduced osmotic pressure and the chain dimensions, etc, at the scaling limit, are described by a single scaled variable, i.e., the reduced concentration. The scaling limit is attained by a solution of infinite chains with a concentration less than a limit and in a good solvent.

In the CSRG, a long chain solution is modeled by a set of Gaussian chains incorporating the δ-function-like two body excluded volume interaction. The Hamiltonian of this "continuous model" is given by

$$H\{\mathbf{C}\} = (1/2)\sum_{i}^{N}\int_{l_0}^{l} d\tau_i (d\mathbf{C}_i/d\tau_i)^2 + (u/2)\sum_{i,j}^{N}\int_{l_0}^{l} d\tau_i \int_{l_0}^{l} d\tau_j' \delta[\mathbf{C}_i(\tau_i) - \mathbf{C}_j(\tau_j')]. \quad (1)$$

In the above, $\mathbf{C}_i(\tau_i)$ represents a continuous chain conformation of the ith chain, τ_i is the distance measured along the chain, u is the excluded volume parameter, N is the number of chains, l is the chain length, and l_0 is the cut off. By extrapolation, our previous numerical experiments of multichain lattice systems arrived at the osmotic pressures or the chain dimensions of the universal forms exhibiting an agreement with the CSRG predictions.[4]

Freed[5] extended the CSRG to the crossover region, where chain lengths are finite and chains are in a solvent of an intermediate quality. He predicted that, in that region, the distance is scaled by the infinite dilution radius of gyration $S(\zeta)$, with ζ being a scaling variable composed of l and u. The solution properties are then governed by ζ and the reduced concentration $c/c^*(\zeta)$, which is the concentration scaled by the overlap concentration $c^*(\zeta)$ evaluated from $S(\zeta)$. He derived universal formulas of the two variables.

In spite of these advances, the author does not feel that the application of the RG idea to long chain solutions has been accepted with well designed critical examination. It should be emphasized that the continuous model Hamiltonian, Eq. (1), will involve some unknown approximations to real long chain solutions. A direct check of the applicability of the RG idea to long chain solutions by using a more realistic model is still of fundamental value. Mere comparison of experimental data with the predictions of the RG mathematics applied on a long chain solution model is not the best for this purpose. Even if the comparison discovers a disagreement of an experiment with an RG prediction, one cannot answer the question as to which of the three, the RG idea, the approximations in the RG mathematics, or the model is responsible for it. In fact, the check was not well presented even in our previous paper.[4]

We have extended our previous experiments[4] to poorer solvent regions and extracted more physical meanings.

In this paper, we study the applicability of the RG idea to our multichain lattice systems. First, we present a typical RG context in multichain language and search for parameter flows by using two RG invariant relations (weak conditions). Next, we examine whether the parameter flows satisfy the essential RG requirements for correlations (strong conditions). The satisfaction will guarantee us the applica-

 0021-9606/88/085095-11$02.10

bility. We find that the applicability is good in the very good solvent region but becomes worse as the solvent condition deteriorates and at the shorter distances. It breaks down in the Θ and the poorer solvent regions. We found two fixed points. But the one in the poor solvent region is fictitious.

In the range where the linearized RG defined by a fixed point in the good solvent region works successfully, we arrived at scaling forms with two or three variables in several fashions. Freed's crossover form[5] corresponds to one of these. Although qualitative, perhaps this is the first experimental confirmation of his prediction. The RG appears to work even in the nonlinear range, i.e., for concentrated solutions outside the semidilute region. As far as we know, this is also the first experimental finding of an RG success in this region.

In the study of the poor solvent region, one adds a three-body term in the continuous model Hamiltonian[6]. The RG parameter flow incorporates this term as a fourth component. Then, in order to be scaling in this region, our lattice model may have to incorporate one more parameter. This problem is as yet unsettled. We need further experiments to understand the affairs in this region.

It has been very optimistically said, that in the scaling limit, the theories and the experiments[7] are in agreement. In reality, however, the distance between the scaling limit and the actual experimental conditions, where chain lengths are finite and solvent conditions are somewhat arbitrary, is never so obvious. We must be more careful for the distance in comparing the experiments with the theories. We hope this paper will also play a role in this respect.

There have been many numerical real space RG studies[8,9] for single chain systems. However, they admit the RG idea without examination.

In the next section, our Monte Carlo simulation technique is described. Comments on the measured quantities are included. In the third section, an RG context in the multichain language is introduced and our method of checking its applicability is mentioned. In the first subsection of the fourth section, the experimental data are analyzed by the proposed scheme. The success and the failure of the RG idea are disclosed. In the following two subsections, the nature of the fixed points we found, and the scaling forms including Freed's one, are discussed. The last section describes summarizing remarks and discusses the RG failure briefly.

II. PROCEDURES

A long chain solution is simulated by a set of arrangements of N self-avoiding chains composed of n contiguous elements (n-mers) on a simple cubic (SC) lattice. The vacant sites are allotted to solvent molecules (1-mer). A nearest-neighbor contact of nonbonded chain elements contributes a potential energy ϵ to the system. The solvent condition is given by $\eta = \exp\{-\epsilon/kT\}$, where kT has the usual meaning. The arrangements are confined within a cubic box made of $L \times L \times L$ sites obeying the periodic boundary condition. The concentration is defined here by $\rho = N/L^3$.

The arrangements were generated by our computer as if they were randomly sampled from a canonical ensemble. To attain this, we adopted Wall *et al.*'s slithering snake technique[10] combined with Metropolis' algorithm[11] as we had done before.[4] The procedure however, is reproduced here for the readers' convenience.

(1) The chains are initially arranged in the box in an arbitrary fashion.

(2) An end element of a chain is randomly chosen. An attempt is made to move this to a randomly chosen adjacent site with the rest of the chain following behind in a snake like fashion.

(3) If this site is occupied by an element, the attempt is abandoned and step 2 is repeated.

(4) If this site is empty and $E_0 > E_1$, where E_0 is the energy of the old arrangement and E_1 is that of the trial one, the movement is accepted as a new arrangement.

(5) If $E_0 < E_1$, then a random number $R(0 < R < 1)$ is chosen. (a) If $R < \exp(E_0 - E_1)/kT$, then the movement is accepted. (b) If $R > \exp(E_0 - E_1)/kT$, the attempt is abandoned.

(6) Steps 2–5 are repeated $N_{\rm rep}$ times. Usually we set $N_{\rm rep} = Nn^2$.

(7) The arrangement after $N_{\rm rep}$ trials is accepted as a sample and is stored in a memory. The procedure goes back to step 2 and generates the next sample.

(8) In the above, the first several samples are rejected.

The number, N_s, of the samples generated for each combination of n, η, and N, was in the range of $5000/N$–$10\,000/N$. Usually, the element fraction, Nn/L^3, did not exceed 0.50. The solvent condition was in a range from 1.0 (athermal) to 1.37. The edge length of the Monte Carlo cell, L (in site number), was eight or more times of the mean-square radius of gyration of the isolated chains in an athermal solvent. These were 20 for 20-mer, 25 for 30-mer, 35 for 40-mer, 45 for 60-mer, and 53 for 80-mer systems. We believe that this choice minimizes the undesirable finite size effects on the statistics.[12]

Because the above procedure generates random sampling from a canonical ensemble, the expectation of the simple mean of a measured quantity for the ith sample M_i, is its canonical average when N_s is large enough, i.e.,

$$\langle M \rangle \to E{:}\langle M \rangle = \sum_i M_i \exp(-E_i/kT) / \sum_i \exp(-E_i/kT), \quad (2)$$

where $\langle M \rangle$ is the simple mean $(1/N_s)\Sigma_i^{N_s} M_i$, E: means the expectation and E_i is the potential energy of the ith arrangement and "i" runs through all the arrangements.

One of the measured quantities was the mean-square radius of gyration, $\langle S^2 \rangle$,

$$\langle S(n,\eta,\rho)^2 \rangle = (1/N_s Nn) \sum_i \sum_k \sum_l (\mathbf{r}_{i,k,l} - \mathbf{g}_{i,k})^2,$$

where $\mathbf{r}_{i,k,l}$ is the position vector of the l th element of the k th chain in the ith sample and $\mathbf{g}_{i,k}$ is that of the mass center of the same chain.

We evaluate a quantity Q_i of an extra n-mer for each sample. This quantity is defined in the following way: Con-

sider the N n-mers arrangement of the ith sample. By adding an extra n-mer, we obtain an $N+1$ n-mers arrangement. There is a number of ways by which this can be done. The definition is

$$Q_i \equiv \sum_q \exp(-U_{i,q}/kT), \tag{3}$$

where $U_{i,q}$ is the potential energy increment of the ith sample by qth way and "q" runs through all of the ways.

By virtue of Eq. (2), the expectation of the simple average of Q_i over samples connects the partition function of $N+1$ n-mers $\Omega(N+1,n,\eta,L)$ with that of N n-mers $\Omega(N,n,\eta,L)$ by

$$\langle Q(N)\rangle \to E:\langle Q(N)\rangle = 2(N+1)\Omega(N+1)/\Omega(N).$$

In the above, the front factor 2 on the right-hand side comes from the symmetricity of a chain. Therefore,

$$(1/N!)2^{-N}\prod_{i=0}^{N-1}\langle Q(i)\rangle \to \Omega(N). \tag{4}$$

The method we adopted to evaluate Q_i was the same as before.[13] In order to make this paper self-contained, a complete explanation is given in the Appendix.

The intra- and the interchain element density distributions around a chain mass center, $P_s(n,\eta,\rho;r)$ and $P_0(n,\eta,\rho;r)$, were simply evaluated by counting the frequency. They are proportional to the corresponding element densities on a site with distance $\mathbf{r}$ from the mass center. These are normalized as

$$\int_{L^3} P_s(r)d^3\mathbf{r} = 1, \tag{5}$$

$$\int_{L^3} P_0(r)d^3\mathbf{r} = N-1. \tag{6}$$

III. THE RENORMALIZATION GROUP IN MULTICHAIN LANGUAGE

Our RG presupposes that an ensemble of chain arrangements on an SC lattice cell with a linear size B and a spacing b is coarse grained into an ensemble of chain arrangements on an SC lattice cell with the linear size B and a spacing b'. By shrinking the coarse-grained lattice, we recover the original spacing b. The linear size then shrinks to B'. The end ensemble is the RG transformed ensemble of the starting one. More precisely, the starting ensemble is a canonical ensemble of the arrangements of N n-mers with the solvent condition η and the transformed ensemble is also canonical but composed of the arrangements of N n'-mers with the solvent condition η', $(n>n')$. The number of chains N is considered as an invariant.

The parameter space is spanned by $1/n$, η, and ρ. An operation of the RG transforms them into

$$(1/n,\eta,\rho) \to (1/n',\eta',\rho'), \tag{7}$$

where the primed quantities are the transformed ones. As usual we call the transformation parameter flow.

The coarse-graining ratio s is defined by

$$s = B/B' = b'/b. \tag{8}$$

We obtain

$$\rho = s^{-3}\rho' \tag{9}$$

since N is invariant.

This paper does not consider the coarse graining from an arrangement to an arrangement but considers that of an ensemble to an ensemble. It does not prescribe a specific coarse-graining method but mentions the legitimate requirements that the RG transformed ensemble should fulfill regardless of the details of the coarse graining. The requirements are condensed in a statement that the correlations before an RG operation will be coupled with those after the operation through a length scale transformation.[14,15] Among the various correlations, we will use the following three, the intra- and the interchain correlations between a chain mass center and respective chain elements and the correlation between chain mass centers. Then, the density distributions defined in the preceding section will be coupled as

$$P_s(1/n,\eta,\rho;r) = s^{-3}P_s(1/n',\eta',\rho';r'), \tag{10a}$$

$$P_0(1/n,\eta,\rho;r) = s^{-3}P_0(1/n',\eta',\rho';r'), \tag{10b}$$

where

$$r = sr'.$$

In the same way, the interchain mass center correlations $G(r)$ will be coupled as

$$G(1/n,\eta,\rho;r) = s^{-6}G(1/n',\eta',\rho';r'). \tag{11}$$

The meaning of that the RG idea is applicable to our multichain systems is that there is a set of parameters or a parameter flow $(1/n,\eta,\rho)\to(1/n',\eta',\rho')$ satisfying Eqs. (10) and (11) simultaneously.

To obtain such flows, we proceed as follows: The second moment of P_s is the mean square radius of gyration:

$$\langle S(1/n,\eta,\rho)^2\rangle = \int d^3\mathbf{r}\, r^2 P_s(1/n,\eta,\rho;r). \tag{12}$$

We obtain Eq. (13) from Eqs. (10a) and (12),

$$s = \langle S(1/n,\eta,\rho)^2\rangle^{1/2}/\langle S(1/n',\eta',\rho')^2\rangle^{1/2}, \tag{13}$$

Combining Eqs. (9) and (13), we get

$$\langle S(1/n,\eta,\rho)^2\rangle^{1/2}\rho = \langle S(1/n',\eta',\rho')^2\rangle^{1/2}\rho'.$$

That is, the quantity defined by

$$X_\rho = \langle S(1/n,\eta,\rho)^2\rangle^{3/2}\rho, \tag{14}$$

is invariant by an RG operation,

$$X_\rho = X'_\rho. \tag{15}$$

Since $\langle S^2\rangle^{3/2}$ is proportional to the average volume spanned by individual chains in the solution, the invariant X_ρ is proportional to the number of chains contained in that volume. Attention that X_ρ is different from the reduced concentration c/c^* or X_0 (see Sec. IV C).

Using Eq. (9) in Eq. (11) and integrating it, we obtain

$$\rho^{-1}\int d^3\mathbf{r}G(r) = \rho'^{-1}\int d^3\mathbf{r}'G(r'). \tag{16}$$

By the relation,[16]

$$\rho^{-1}\int d^3\mathbf{r}G(r) = kT\left(\frac{\partial\pi}{\partial\rho}\right)^{-1}.$$

Equation (16) means that

$$\frac{\partial\pi}{\partial\rho}=\left(\frac{\partial\pi}{\partial\rho}\right)'. \tag{17}$$

For convenience, we convert $\langle Q\rangle$ to a form independent of L,

$$\langle\omega\rangle\equiv\langle Q\rangle/L^3.$$

Then, after applying an elementary procedure to Eq. (4) we obtain

$$(kT)^{-1}\left(\frac{\partial\pi}{\partial\rho}\right)=1-\left(\frac{\rho d\ln\langle\omega\rangle}{d\rho}\right). \tag{18}$$

Equations (17) and (18) tell us that the quantity Y defined by

$$Y=\frac{\rho d\ln\langle\omega\rangle}{d\rho} \tag{19}$$

is invariant,

$$Y=Y'. \tag{20}$$

This means the same thing as Eq. (17), i.e., that the osmotic compressibility is an RG invariant.

In what follows, we tentatively determine the flows from the rule that X_ρ and Y are invariant (weak conditions). Remember that X_ρ and Y can be evaluated from our measured quantities and the manipulation from Eq. (10) to Eq. (20) needs no approximation. Then, we examine the satisfaction of Eqs. (10a) and (10b) by the same flows (strong conditions). Simultaneous satisfaction authorizes the flows and guarantees us the applicability of the RG. The omission of the examination by other correlations will not yield important misunderstandings.

The success of the RG in constructing the universal relations depends on identifying a fixed point for which $1/n=1/n'=1/n^*$, $\eta=\eta'=\eta^*$, $\rho=\rho'=\rho^*$. Equations (7) and (9) indicate at once

$$1/n^*\to 0, \tag{21a}$$

$$\rho^*\to 0. \tag{21b}$$

The estimation of η^* is discussed in the next section.

IV. RESULTS AND DISCUSSION

A. Parameter flows

1. An illustrative example in concentrated solutions

The values of X_ρ and Y were evaluated from the measured quantities $\langle S^2\rangle$ and $\langle Q\rangle$. The evaluations were accomplished by numerical manipulations including differentiation and interpolation. We plot Y against X_ρ by using a group of systems having a fixed set of n and η but of various ρ's.

Figure 1 shows several plottings. Because X_ρ and Y are invariant in an RG operation (weak condition), each of the crossings of the plottings designates a candidate of an RG couple or a parameter flow. For example the crossing marked by an arrow in the figure designates the flow $(1/80, 1.13, 310/53^3)\to(1/30, 1.20, 189/25^3)$.

Following the scheme in the preceding section, we examine the simultaneous satisfaction of Eqs. (10a) and (10b), the strong conditions, with the same flow. As shown in Fig. 2, where the scales are renormalized to the 30-mer system, the satisfaction is fairly good. The applicability in this case is thus confirmed.

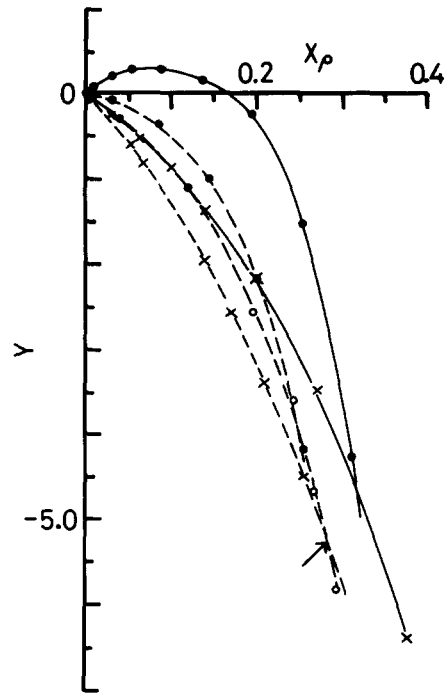

FIG. 1. Plottings of Y vs X_ρ for several groups of the systems. (-×-): $n=80$, $\eta=1.13$, various ρ's in the range from 0. to $310/53^3$, (—×—): $n=80$, $\eta=1.20$, various ρ's in the range from 0. to $558/53^3$, (-O-): $n=30$, $\eta=1.20$, various ρ's in the range from 0 to $208/25^3$, (-●-): $n=20$, $\eta=1.26$, various ρ's in the range from 0. to $200/20^3$, (—●—): $n=20$, $\eta=1.37$, various ρ's in the range from 0. to $240/20^3$.

It is noticeable that this example is the RG in concentrated solutions outside the semidilute region as will be described later. Notice the site fractions, Nn/L^3, in the above amount to 0.167 and 0.363.

We made a lot of plottings of Y vs X_ρ. We found the

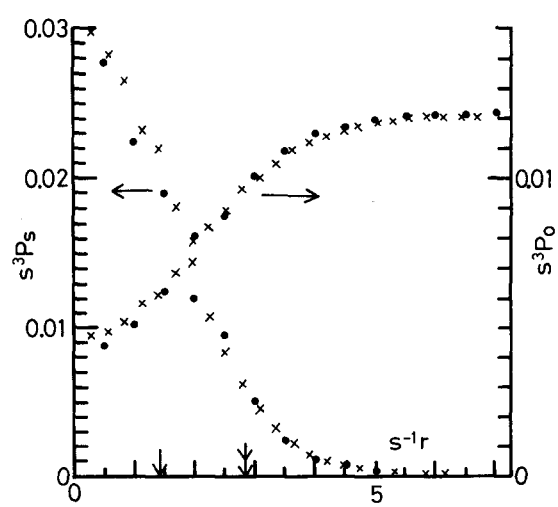

FIG. 2. Examination of Eqs. (10a) and (10b) by the systems designated by the arrow in Fig. 1. s^3P_s vs $s^{-1}r$ and s^3P_0 vs $s^{-1}r$. (×): $n=80$, $\eta=1.13$, $\rho=310/53^3$, $X_\rho=0.280$, (●): $n=30$, $\eta=1.20$, $\rho=189/25^3$, $X_\rho=0.281$. The arrow indicates $s^{-1}r=\langle S(n=30)^2\rangle^{1/2}/2$ and the double arrow indicates two times this distance.

flows which play roles in establishing the scaling forms. We show several examples.

2. The very good solvent region

Figure 3 shows three plottings of Y vs X_ρ coming from the three groups of the systems [$n = 80$, $\eta = 1.00$, and various ρ's in the range from 0 to $465/53^3$], [$n = 60$, $\eta = 1.033$, and various ρ's in the range from 0 to $212/45^3$], and [$n = 20$, $\eta = 1.08$, and various ρ's in the range from 0 to $223/20^3$]. The three plottings fall nearly on a common curve when X_ρ is not so large, $\sim X_\rho < 0.15$. The weak condition designates the flows $(1/80, 1.00, \rho) \rightarrow (1/60, 1.033, \rho') \rightarrow (1/20, 1.08, \rho'')$. In this case the value of ρ is arbitrary provided it satisfies $X_\rho < 0.15$. For an arbitrary starting ρ, there is a ρ' and a ρ''. This is in contrast to the first example (Fig. 1) in which the flow $\rho \rightarrow \rho'$ is uniquely specified.

Figure 4 shows the examination of the flows by using the strong conditions. In the figure, the scales are renormalized to the 20-mer systems. In Figs. 4(a) and 4(b), s^3P_0 at two specified distances, $\langle S(n, \eta, \rho)^2\rangle^{1/2}/2$ and two times this, are plotted against X_ρ. In the evaluation of the coarse-graining ratio given by Eq. (13), the denominators with $n = 20$, $\eta' = 1.08$, and some ρ's were estimated through interpolation. The points are on respective master curves, indicating a simultaneous satisfaction. Figure 4(c) shows a whole comparison of s^3P_s vs s^{-1}r and s^3P_s vs $s^{-1}r$. It demonstrates fairly good simultaneous satisfaction. The RG applicability is guaranteed.

We notice that the solvent condition becomes poorer by the RG. We call this region the very good solvent region.

In the present example and also in the subsequent ones, the simultaneous satisfaction of the intrachain distributions encounters no serious failure. The description will mainly concern with the interchain distributions.

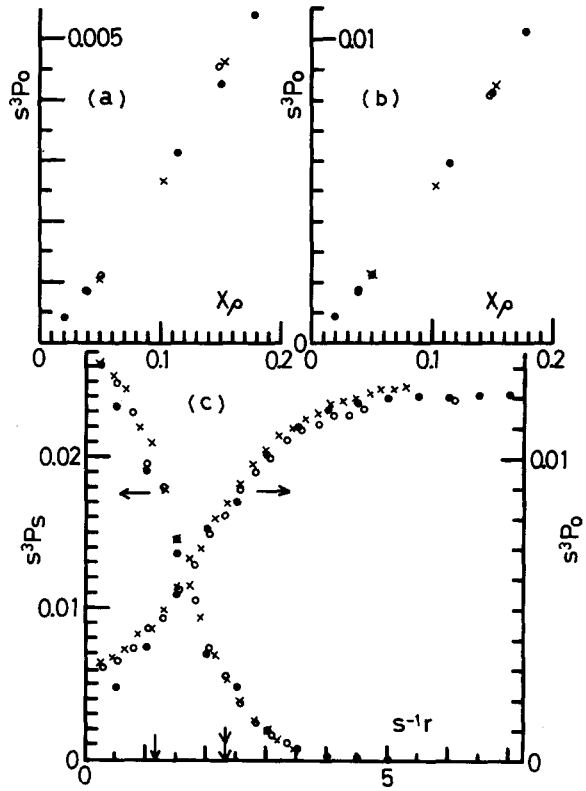

FIG. 4. Examination of Eqs. (10a) and (10b) by the systems referred to in Fig. 3. The scales are renormalized to the 20-mer systems. The symbols are the same as in Fig. 3. (a) $s^3P_0(r = \langle S^2\rangle^{1/2}/2)$ vs X_ρ. (b) $s^3P_0(r = \langle S^2\rangle^{1/2})$ vs X_ρ. (c) Comparison of the distributions s^3P_s vs $s^{-1}r$ and s^3P_0 vs $s^{-1}r$, for the systems having a nearly common value of X_ρ. The half-bell shaped plots are for P_s. The half-dish shaped plots are for P_0. For the 80-mer system, $\rho = 140/53^3$, $X_\rho = 0.153$, for the 60-mer system, $\rho = 144/45^3$, $X_\rho = 0.148$, for the 20-mer system, $\rho = 96/20^3$, $X_\rho = 0.150$. The arrow indicates $s^{-1}r = \langle S(n = 20)^2\rangle^{1/2}/2$ and the double arrow indicates two times this distance.

3. The good solvent fixed point

Figure 5 shows the three plottings of Y vs X_ρ coming from the three groups of the systems [$n = 80$, $\eta = 1.13$, and

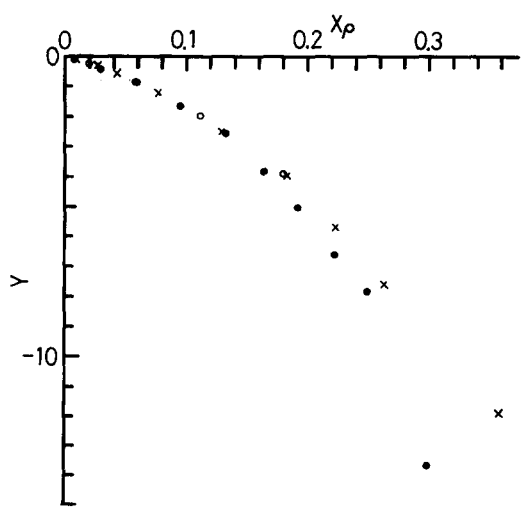

FIG. 3. Plottings of Y vs X_ρ for the systems in the very good solvent region. (×): $n = 80$, $\eta = 1.00$, various ρ's in the range from 0. to $465/53^3$, (○): $n = 60$, $\eta = 1.033$, various ρ's in the range from 0. to $212/45^3$, (●): $n = 20$, $\eta = 1.08$, various ρ's in the range from 0. to $233/20^3$.

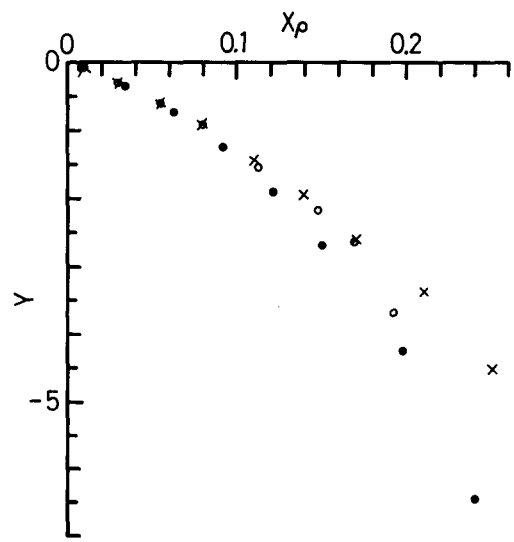

FIG. 5. Plottings of Y vs X_ρ for the systems with $\eta = 1.13$ (the good solvent fixed point). (×): $n = 80$, $\eta = 1.13$, various ρ's in the range from 0. to $310/53^3$, (○): $n = 40$, $\eta = 1.13$, various ρ's in the range from 0. to $214/35^3$, (●): $n = 20$, $\eta = 1.13$, various ρ's in the range from 0. to $170/20^3$.

various ρ's in the range from 0 to $310/53^3$], [$n=40$, $\eta=1.13$, and various ρ's in the range from 0 to $214/35^3$], and [$n=20$, $\eta=1.13$, and various ρ's in the range from 0 to $170/20^3$]. They fall on a common curve when $\sim X_\rho < 0.7$. The weak condition designates parameter flows of $(1/80, 1.13, \rho) \rightarrow (1/40, 1.13, \rho') \rightarrow (1/20, 1.13, \rho'')$ for arbitrary ρ's satisfying $X_\rho < 0.15$.

Figure 6 shows the examination using the strong conditions. We see again fairly good simultaneous satisfaction although the deviations at the shortest distances are nonnegligible.

It is noticeable that the solvent condition $\eta=1.13$ is invariant by the RG. The solvent condition is a fixed point solvent condition. We denote it by η_g^* and call this fixed point the good solvent fixed point. The η_g^* value is a little different from our previous one 1.1[4] but is more precise. It is also noteworthy that this solvent condition is not athermal.

4. The intermediate solvent region

Figure 7 shows the three plottings of Y vs X_ρ coming from the three groups of the systems [$n=80$, $\eta=1.20$, and various ρ's in the range from 0 to $275/53^3$], [$n=40$, $\eta=1.19$, and various ρ's in the range from 0 to $249/35^3$], and [$n=20$, $\eta=1.185$, and various ρ's in the range from 0 to $120/20^3$]. The weak condition designates the parameter flows $(1/80, 1.20, \rho) \rightarrow (1/40, 1.19, \rho') \rightarrow (1/20, 1.185, \rho'')$ for any ρ satisfying $X_\rho < 0.05$.

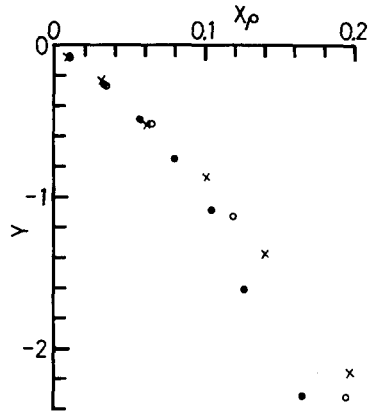

FIG. 7. Plottings of Y vs X_ρ for the system in the intermediate solvent region. (×): $n=80$, $\eta=1.20$, various ρ's in the range from 0. to $272/53^3$, (○): $n=40$, $\eta=1.19$, various ρ's in the range from 0. to $249/35^3$, (●): $n=20$, $\eta=1.185$, various ρ's in the range from 0. to $120/20^3$.

Figure 8 shows the examination of the flows using the

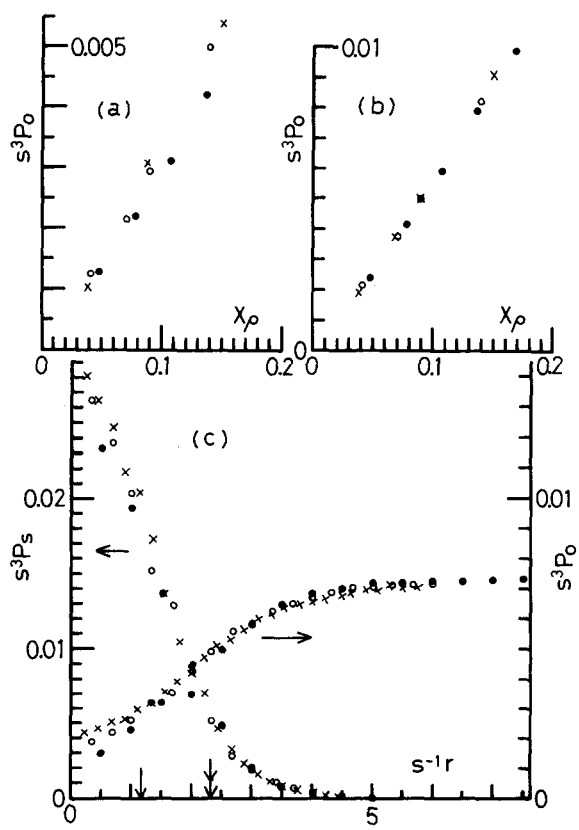

FIG. 6. Examination of Eqs. (10a) and (10b) by the systems with $\eta=1.13$ referred to in Fig. 5. The scales are renormalized to the 20-mer system. The symbols are the same as in Fig. 5. (a) $s^3P_0(r=\langle S^2\rangle^{1/2}/2)$ vs X_ρ. (b) $s^3P_0(r=\langle S^2\rangle^{1/2})$ vs X_ρ. (c) Comparison of the distributions s^3P_s vs $s^{-1}r$ and s^3P_0 vs $s^{-1}r$, for the systems having a nearly common value of X_ρ. For the 80-mer system, $\rho=90/53^3$, $X_\rho=0.0878$, for the 40-mer system, $\rho=90/35^3$, $X_\rho=0.0890$, for the 20-mer system, $\rho=58/20^3$, $X_\rho=0.0911$. The arrow and the double arrow indicate the same things as in Fig. 4.

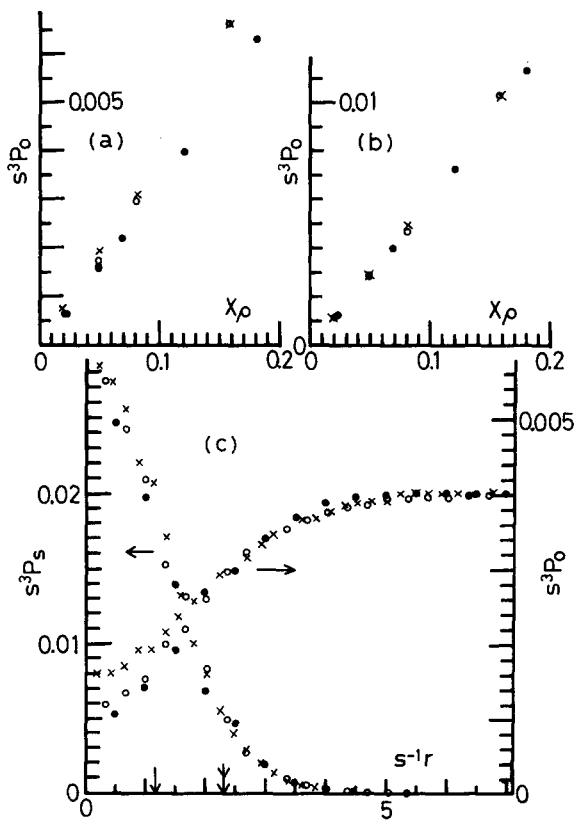

FIG. 8. Examination of Eqs. (10a) and (10b) by the systems referred to in Fig. 7. The scales are renormalized to the 20-mer systems. The symbols are the same as in Fig. 7. (a) $s^3P_0(r=\langle S^2\rangle^{1/2}/)$ vs X_ρ. (b) $s^3P_0(r=\langle S^2\rangle^{1/2}/)$ vs X_ρ. (c) Comparison of the distributions s^3P_s vs $s^{-1}r$ and s^3P_0 vs $s^{-1}r$, for the systems having a nearly common value of X_ρ. For the 80-mer system, $\rho=56/53^3$, $X_\rho=0.0494$, for the 40-mer system, $\rho=52/45^3$, $X_\rho=0.0490$, for the 20-mer system, $\rho=32/20^3$, $X_\rho=0.0487$. The arrow and the double arrow mean the same things as in Fig. 4.

strong conditions. The simultaneous satisfaction is good when the distance is longer than the mean-square radius of gyration but is not good when it is shorter than that.

The solvent condition becomes better by the RG. We call this region the intermediate solvent region.

5. The poor solvent region

Figure 9 includes the plottings of Y vs X_ρ obtained from the systems with poor solvent conditions.

First, notice the three plottings connected by dotted lines which come from the three groups [$n = 80$, $\eta = 1.32$, and various ρ's in the range from 0 to $192/53^3$], [$n = 40$, $\eta = 1.32$, and various ρ's in the range from 0 to $126/35^3$], and [$n = 20$, $\eta = 1.32$, and various ρ's in the range from 0 to $78/20^3$]. The plottings suggest the parameter flows $(1/80, 1.32, \rho) \rightarrow (1/40, 1.32, \rho') \rightarrow (1/20, 1.32, \rho'')$ for arbitrary ρ's satisfying $X_\rho < 0.02$.

The solvent condition $\eta = 1.32$ is invariant. The solvent condition appears to be another fixed point solvent condition η_p^*. For the moment we will call this the poor solvent fixed point. However, the examination using the strong condition is quite unsatisfactory as is shown in Fig. 10. This means the failure of the applicability of the RG to our multichain systems.

Secondly, notice the three plottings in Fig. 9 connected by continuous lines. They come from the three groups [$n = 80$, $\eta = 1.35$, and various ρ's in the range from 0 to $145/53^3$], [$n = 40$, $\eta = 1.355$, and various ρ's in the range from 0 to $26/35^3$], and [$n = 20$, $\eta = 1.36$, and various ρ's in the range from 0 to $50/20^3$]. That the flow lines suggested by these plottings are fictitious is made clear by the examination shown in Fig. 11.

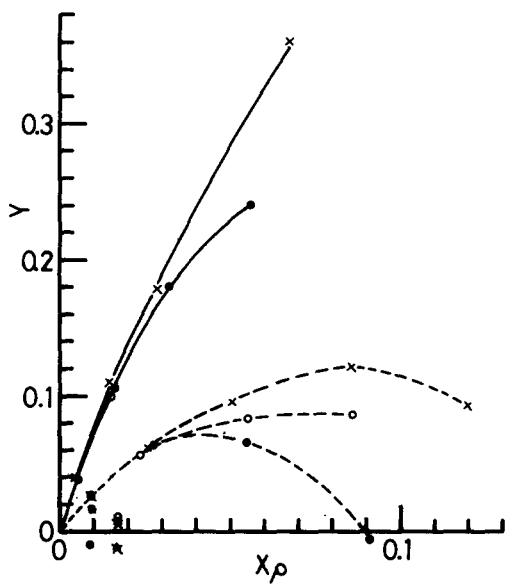

FIG. 9. Plottings of Y vs X_ρ for the systems in the poor solvent region. Points just below the abscissa; (×): $n = 80$, $\eta = 1.29$, $\rho = 45/53^3$, (○): $n = 60$, $\eta = 1.29$, $\rho = 43/45^3$, (●): $n = 20$, $\eta = 1.28$, $\rho = 22/20^3$. Points just above the abscissa; (×): $n = 80$, $\eta = 1.30$, $\rho = 47/53^3$, (△); $n = 60$, $\eta = 1.30$, $\rho = 44/45^3$, (○): $n = 40$, $\eta = 1.30$, $\rho = 41/35^3$, (●): $n = 20$, $\eta = 1.30$, $\rho = 12/20^3$. (-×-): $n = 80$, $\eta = 1.32$, various ρ's in the range from 0. to $192/53^3$, (-○-): $n = 40$, $\eta = 1.32$, various ρ's in the range from 0. to $126/35^3$, (-●-): $n = 20$, $\eta = 1.32$, various ρ's in the range from 0. to $78/20^3$. (—×—): $n = 80$, $\eta = 1.350$, various ρ's in the range from 0. to $145/53^3$, (—○—): $n = 40$, $\eta = 1.355$, various ρ's in the range from 0. to $26/35^3$, (—●—): $n = 20$, $\eta = 1.360$, various ρ's in the range from 0 to $50/20^3$.

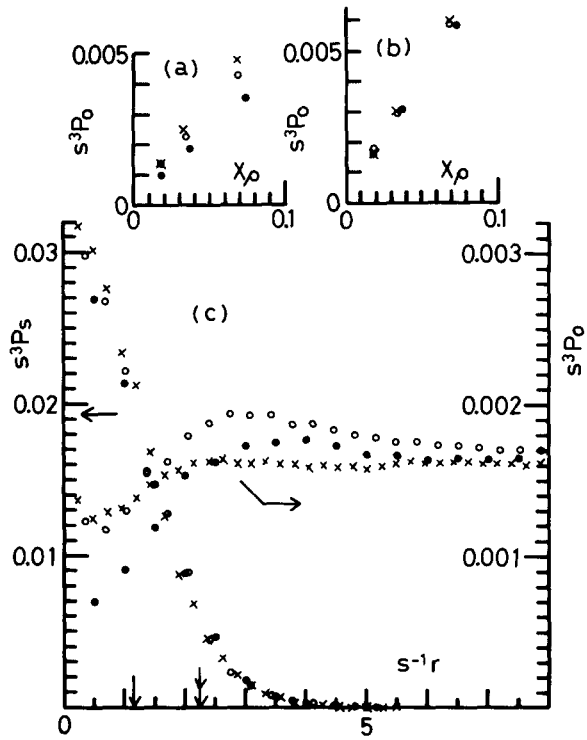

FIG. 10. Examination of Eqs. (10a) and (10b) by the systems with $\eta = 1.32$ referred to in Fig. 9. The scales are renormalized to the 20-mer systems. The symbols are the same as in Fig. 9. (a) $s^3P_0(r = \langle S^2\rangle^{1/2}/2)$ vs X_ρ. (b) $s^3P_0(r = \langle S^2\rangle^{1/2})$ vs X_ρ. (c) Comparison of the distributions s^3P_s vs $s^{-1}r$ and s^3P_0 vs $s^{-1}r$, for the system having a nearly common value of X_ρ. For the 80-mer system, $\rho = 26/53^3$, $X_\rho = 0.0181$, for the 40-mer system, $\rho = 23/35^3$, $X_\rho = 0.0187$, for the 20-mer system, $\rho = 13/20^3$, $X_\rho = 0.0183$. The arrow and the double arrow mean the same things as in Fig. 4.

6. The θ point

Here, we will show another indication of the failure of the application of the RG.

Notice the points in Fig. 9 which are not connected by lines. Since the slope of Y vs X_ρ at the origin is proportional to the second virial coefficient (see below), the solvent conditions of these points are near to the θ solvent condition η_θ at which the second virial coefficient vanishes.

By interpolating the data (some of them are omitted in the figure) we estimate η_θ as 1.287 for $n = 20$, 1.292 for $n = 40$, and 1.297 for $n = 80$. We estimate $\eta_\theta(n \rightarrow \infty)$ as 1.305 ± 0.002 through a simple extrapolation. If the apparent fixed point $\eta_p^*(= 1.32 \pm 0.003)$ is a true one, η_p^* should coincide with $\eta_\theta(n \rightarrow \infty)$ because of its repulsive nature (see below). The observed small, but finite, difference between them demonstrates the indication of the failure of the RG idea. Notice that the failure is not remedied by a simple increase of chain length.

Our $\eta_\theta(n)$'s are in close agreement with those obtained by Janssens *et al.*'s.[17] They are 1.280 for $n = 20$, 1.293 for $n = 40$, 1.295 for $n = 80$, and 1.309 ± 0.001 for $n \rightarrow \infty$. Bruns's estimation is also 1.309.[23]

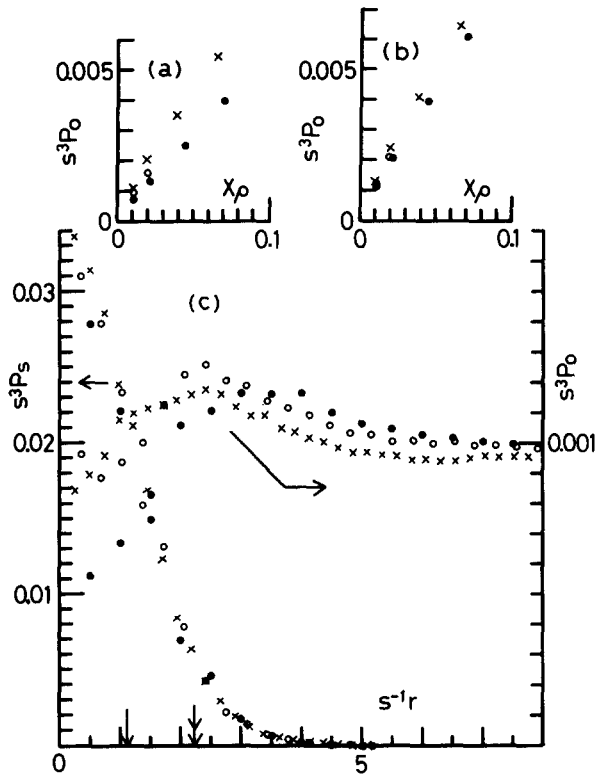

FIG. 11. Examination of Eqs. (10a) and (10b) by the systems referred to in Fig. 9. The scales are renormalized to the 20-mer systems. (×): $n = 80$, $\eta = 1.350$, (○): $n = 40$, $\eta = 1.355$, (●): $n = 20$, $\eta = 1.360$. (a) $s^3P_0(r = \langle S^2\rangle^{1/2}/2)$ vs X_ρ. (b) $s^3P_0(r = \langle S^2\rangle^{1/2})$ vs X_ρ. (c) Comparison of the distribtuions s^3P_s vs $s^{-1}r$ and s^3P_0 vs $s^{-1}r$, for the systems having a nearly common value of X_ρ. For the 80-mer system, $\rho = 16/53^3$, $X_\rho = 0.0102$, for the 40-mer system, $\rho = 14/35^3$, $X_\rho = 0.0108$, for the 20-mer system, $\rho = 8/20^3$, $X_\rho = 0.0107$. The arrow and the double arrow mean the same things as in Fig. 4.

7. Addenda to Sec. IV A

(1) Since two different analytic functions never coincide throughout an interval, the apparent accumulation of the points on a curve in the Y–X_ρ plane does not mean a true coincidence of Y vs X_ρ curves. In this sense, the parameter flows found in the Secs. from IV A 2 to IV A 4 involve some approximations.

(2) The flow lines near the good solvent fixed point indicate that the fixed point is attractive along the solvent condition axis. In the same way the apparent poor solvent fixed point is repulsive. The latter is consistent with the tricriticality picture in this region.[1]

We will continue the RG analysis still further because the RG idea works well in the very good solvent region and does not work badly even in the intermediate solvent region.

B. The linearized RG and the critical exponents

Figure 5 shows that when $\eta = \eta_g^*$, the flow lines are confined in the $\eta = \eta_g^*$ plane. This finding and an obvious physical reasoning tell us that the lines ($1/n = 0$, $\eta = \eta_g^*$) and ($\eta = \eta_g^*$, $\rho = 0$) are flow lines. It is obvious that the line ($1/n = 0, \rho = 0$) is a flow line. These lines are, therefore, the principal axes of the linearized RG around the good solvent fixed point. An established RG[14] context then asserts that near the fixed point,

$$1/n = s^x(1/n'), \tag{22a}$$

$$\eta - \eta_g^* = s^y(\eta' - \eta_g^*), \tag{22b}$$

and

$$\rho = s^z\rho'. \tag{22c}$$

Equation (22a) is, by virtue of Eqs. (9) and (13), equivalent to

$$\langle S(n,\eta_g^*,0)^2\rangle \propto n^{2\nu} \tag{23}$$

with

$$x = -1/\nu.$$

It is of value for us to confirm the consistency of these equations with our numerical experiments. Among them, Eq. (22c) requires no attention since it is the same as Eq. (9). Of course, Eq. (23) has been well established.[1] The least-mean-square method gives the value of $\nu = 0.575$ by using the data of chains with n in the range from 60 to 180. The fact that this value is nonnegligibly smaller than the theoretical one 0.588 may require further investigation.

Unfortunately, confirmation of Eq. (22b) is at a halfway stage because of the scattering of the points and the increasing difficulty in getting the data for longer chains. The ambiguity involved in the value of η_g^* ($= 1.13 \pm 0.005$) makes the situation worse. In spite of this, at present, supported by the consistency in this region, we believe that Eq. (22b) does hold.

C. The scaling forms

The simultaneous satisfaction disclosed in the Sec. IV A means that the correlations or the density distributions are governed by X_ρ, $Y[= 1 - (1/kT)\partial\pi/\partial\rho]$ and the distance is scaled by $\langle S(n,\eta,\rho)^2\rangle$ We thus arrive at

$$P_{s_0}(n,\eta,\rho;r) = S_\rho^{-3}\mathscr{P}_{s_0}^{(1)}[X_\rho,(1/kT)\partial\pi/\partial\rho;r/S_\rho] \tag{24}$$

with the abbreviation S_ρ for $\langle S(n,\eta,\rho)^2\rangle^{1/2}$.

The major difference between Eq. (24) and Freed's prediction cited in the Introduction is in the fact that while the right-hand side of Eq. (24) is a function of variables measured by the solution under consideration, the variables in the latter are scaled by the quantities at vanishing concentration solutions. We show that the linearized RG makes the two forms mutually equivalent.

Equations (22) mean the mutual independence of the components of parameter flows. Therefore, for a given coarse-graining ratio, if $(1/n, \eta, \rho) \to (1/n', \eta', \rho')$ then $(1/n, \eta, 0) \to (1/n', \eta', 0)$ and vice versa. The coarse-graining ratio is given in two equivalent ways,

$$s = \langle S(n,\eta,\rho)^2\rangle^{3/2}/\langle S(n',\eta',\rho')^2\rangle^{3/2}$$
$$= \langle S(n,\eta,0)^2\rangle^{1/2}/\langle S(n',\eta',0)^2\rangle^{1/2}.$$

The latter and Eq. (9) tells us that the variable

$$X_0 = \langle S(n,\eta,0)^2\rangle^{3/2}\rho, \tag{25}$$

which is the same quantity of Freed's reduced concentration $c/c^*(\zeta)$, is invariant,

$$X_0 = X_0'. \tag{26}$$

For the vanishing concentration system, the expansion,

$$Y = Y)_{X_\rho = 0} + \left(\frac{\partial Y}{\partial X_\rho}\right)_{X_\rho = 0} X_\rho$$

means that $(\partial Y/\partial X_\rho)_{X_\rho = 0}$ is invariant. Denoting

$$\psi = \left(\frac{\partial Y}{\partial X_\rho}\right)_{X_\rho = 0}, \tag{27}$$

we can use the relation

$$\psi = \psi' \tag{28}$$

to determine the flows. Here, -2ψ is the penetration function since

$$\left(\frac{\partial Y}{\partial X_\rho}\right)_{X_\rho = 0} = -(1/2)A_2/\langle S(n,\eta,0)^2\rangle^{3/2},$$

where A_2 is the second virial coefficient.

The variable ψ is determined solely by chain length and solvent condition and just corresponds to Freed's scaling variable ζ. A flow line in our parameter space can be identified by either of (X_ρ, Y) or (X_0, ψ). Thus,

$$X_\rho = X_\rho(X_0,\psi), \tag{29a}$$

$$Y = Y(X_0,\psi). \tag{29b}$$

Rewriting Eq. (29a), we get the two scaled variables form for the reduced chain dimension,

$$\langle S(n,\eta,\rho)^2\rangle/\langle S(n,\eta,0)^2\rangle = f(X_0,\psi). \tag{30}$$

Putting Eqs.(29a), (29b), and (30) in Eq.(24), we arrive at the scaling form in Freed's fashion

$$P_{\vec{0}} = S_0^{-3}\mathscr{P}_{\vec{0}}^{(2)}(X_0,\psi; r/S_0) \tag{31}$$

with the abbreviation S_0 for $\langle S(n,\eta,0)^2\rangle^{1/2}$.

We can get scaling forms with different variables in several fashions from Eqs.(22). For example, eliminating the coarse-graining ratio from them, we find that the variables $n^{-\nu y}(\eta - \eta_g^*)$ and $n^{3\nu}\rho$ are invariant. This leads us to the formulation

$$P_{\vec{0}} = n^{-3\nu}\mathscr{P}_{\vec{0}}^{(3)}(n^{3\nu}\rho, n^{-\nu y}(\eta - \eta_g^*); rn^{-\nu}). \tag{32}$$

Figure 12 shows the plottings by Eq.(29a) for the systems having $\eta = \eta_g^*$. The plottings for the systems in the very good solvent region and those in the intermediate solvent region overlap with the points in the figure and are omitted.

The plottings in the form of Eq.(29b) by using the help of Fig. 12 did not differ much from those of Y vs X_ρ shown in Figs. 1, 3, and 5 and are not shown here. In fact, they are, by virtue of Eqs.(18) and (19), Freed's fashion scaling forms of $\partial\pi/\pi\rho$. Although qualitative, this is the first experimental confirmation of his prediction.

Figure 13 shows the plottings of the reduced chain dimension in the form of Eq.(30).

Numerical comparison of these curves with the theory might be important but was not performed. The theoretical formulas are too complicated for us to calculate immediately and our data are not yet so abundant.

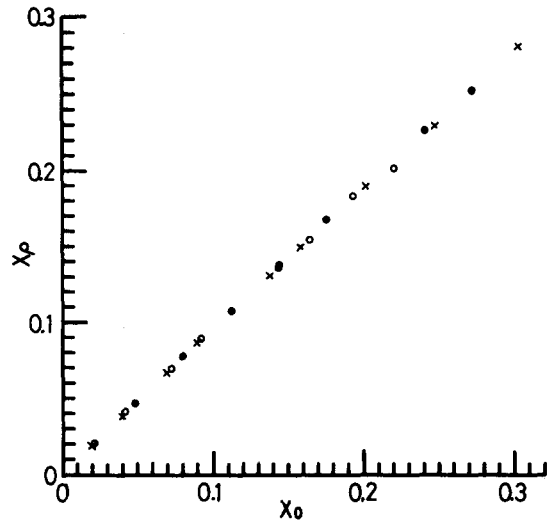

FIG. 12. Plottings of X_ρ vs X_0, for the systems with the solvent condition at the good solvent fixed point. (×): $n = 80$, $\eta = 1.13$, and various ρ's in the interval from 0. to $10/53^3$, (○): $n = 40$, $\eta = 1.13$, and various ρ's in the interval from 0. to $214/35^3$, (●): $n = 20$, $\eta = 1.13$, and various ρ's in the interval from 0. to $170/20^3$.

From their experiments of polystyrene solutions in toluene and in MEK, Wiltzius *et al.* concluded that the equilibrium properties are governed solely by the concentration multiplied by the second virial coefficient.[19] This means that our scaling formulation such as Eq.(29b) is further reduced to as

$$Y = \tilde{Y}(\psi X_0).$$

That is, the equilibrium properties are doubly scaled. Although the combination of the plottings in Figs. 3, 5, and 7 appears to demonstrate some supporting features, it is a matter of careful examination and is put aside in this paper.

Because of the attractive nature of the good solvent fixed point, solutions of infinitely long chains in solvent regions better than intermediate are universally described by a single variable X_0 when they are dilute enough. As reported, the

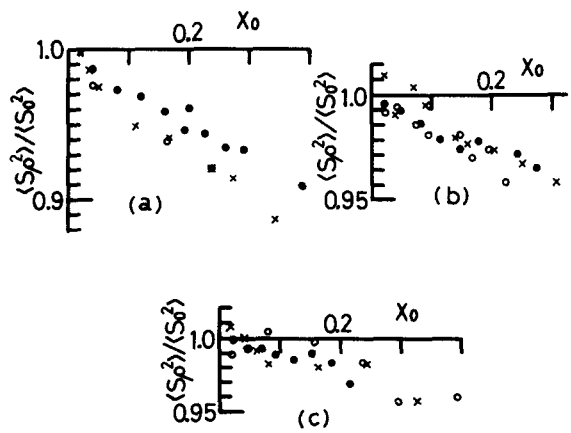

FIG. 13. Plottings of $\langle S(n,\eta,\rho)^2\rangle/\langle S(n,\eta,0)^2\rangle$ vs X_0 for three solvent regions. (a) Plottings for the systems in the very good solvent region referred to in Fig. 3. (b) Plottings for the systems with the solvent condition at the good solvent fixed point referred to in Fig. 5. (c) Plottings for the systems in the intermediate solvent region referred to in Fig. 7. The symbols mean the same things as those in the corresponding figures.

agreement of our osmotic pressures or chain dimensions vs X_0 relations with the theory at the scaling limit is satisfactory.[4] The value of 2ψ at the good solvent fixed point was 10.3 ± 0.1 which is in close agreement with the theoretical one 10.3 predicted by Oono *et al.*[20]

V. SUMMARIZING REMARKS AND COMMENTS ON THE RG FAILURE

A scheme to study the applicability of the RG idea to multichain lattice systems is constructed. The RG idea is successfully applicable to our multichain lattice systems in the very good solvent region but is unsuccessful with increasing deterioration of the solvent conditions. In the regions where the RG works successfully, the correlations are governed by the osmotic compressibility and the distance scaled by the radius of gyrations of the chains in the solution under consideration.

The universality and the crossover scaling predicted by the CSRG correspond to the affairs in our linearized RG around the good solvent fixed point. In the region where the linearized RG works, the correlations are equally governed by the variables scaled by the quantities measured at vanishing concentration. There is a good correspondence between this region and the dilute and semidilute regions in the usual polymer terminology. There is also a good numerical coincidence of our data with the theoretical predictions. It is interesting to note that the solvent condition η in our model behaves similarly to the excluded volume parameter u in the continuous model although they are differently defined. It should be remembered that the solvent condition at ourgood solvent fixed point is not athermal. Unfortunately the value of the critical exponent $\nu = 0.575$) did not agree with the theoretical one calculated for an isolated chain 0.588.

The RG in the nonlinear range corresponds to the RG for solutions outside of the semidilute region. The RG in this region has not been a close target of recent quantitative studies. Although the number of the example is only one, our confirmation may invoke some interest in the field.

The RG failure in the poor solvent regions reminds us of Kremer *et al.*'s numerical work[21] for single chains in which failure of the theoretical scaling rules in the Θ region was reported.

The failure may be attributed to the lack of longer chain data.[21] However, the nature of the failure described in Sec. IV A 6 is not consistent with this view. Another view attributes the RG failure to the inherent nature of our multichain lattice systems.

Through converting the lattice model to the continuous model the recent work of Freed's group found some contributions of the nearest-neighbor interaction in the former model to the three body term in the latter model.[22] The two body and the three body term in the continuous model vanish simultaneously at the poor solvent fixed point. We notice that, in the lattice model, this will not be accomplished by a simple adjustment of the nearest-neighbor interaction.

If the introduction of one more parameter in our multichain lattice systems could accomplish the above fixed point requirement, then the RG failure will be remedied. Many experiments are needed to understand the affairs in the poor solvent regions.

ACKNOWLEDGEMENTS

This work used the computer system HITAC M-200H in the Computer Center of the Institute of Molecular Science. It was partly supported by the Grant in Aid for Cooperative Research by the Japanese Ministry of Education, Science, and Culture in 1985(No. 60303018). The author thanks Lecturer J. G. Toff for his help in improving the English in the manuscript.

APPENDIX

We add an extra n-mer onto the ith arrangement ($i = 1, 2, \ldots$) of N n-mers with the solvent condition η by the following procedure. Our task is to get the sum of the Boltzmann weights associated with all the allowable ways, $Q_i(N)$, Eq. (3).

(1) The first element of an extra n-mer is put on a site randomly chosen from the Monte Carlo cell. The weight at this step, $W_{i,\alpha,1}$ ($\alpha = 1,2,\ldots$, see below), is $L^3\eta^{z(\alpha,1)}$ if the site is empty and is a neighbor to $z(\alpha,1)$ occupied sites. The weight $W_{i,\alpha,1}$ is 0 if the site is occupied by an element.

(2) Let this site be a neighbor to $t(\alpha,1)$ empty sites.

(3) The second element is put onto a site randomly chosen from the empty sites. The weight at this step $W_{i,\alpha,2}$ is $W_{i,\alpha,1}\ t(\alpha,1)\ \eta^{z(\alpha,2)}$ if this site is a neighbor to $z(\alpha,2)$ occupied sites. If $t(\alpha,1) = 0$, the weight is 0.

(4) Let this site be a neighbor to $t(\alpha,2)$ empty sites.

(5) The steps like 3 and 4 are repeated until the nth element is put on the cell. We then get the weight $W_{i,\alpha,n}$ as

$$W_{i,\alpha,n} = L^3\left\{\prod_{k=1}^{N-1} t(\alpha,k)\right\}\eta^{\Sigma_k z(\alpha,k)}. \tag{A1}$$

The attained configuration is labeled by α.

(6) Steps 1–5 are repeated N_{ext} times on the same arrangement.

Thus, we get a set of weights $W_{i,\alpha,n}$ ($\alpha = 1,2,\ldots N_{\text{ext}}$). We can prove that the simple mean of $W_{i,\alpha,n}$ over the set is expected to approach the desired quantity, Q_i. (This proof was omitted in our previous paper.[13])

In principle we can attain any of the allowable configurations, α, by the probability p_α,

$$p_\alpha = 1/\left\{L^3\prod_{k=1}^{N-1} t(\alpha,k)\right\} \tag{A2}$$

with

$$\sum_\alpha p_\alpha = 1. \tag{A3}$$

The simple mean of the obtained weights

$$\langle W_{i,\alpha,n}\rangle = \left(\sum_\alpha W_{i,\alpha,n}\right)\Big/ N_{\text{ext}}$$

converges to its expectation for large N_{ext} as

$$\langle W_{i,\alpha,n}\rangle \to \sum_\alpha W_{i,\alpha,n}p_\alpha / \sum_\alpha p_\alpha, \tag{A4}$$

where α runs through all configurations. By using Eqs.(A1), (A2), and (A3) we get from Eq.(A4),

$$\langle W_{i,\alpha,n} \rangle \to \sum_{\alpha} \eta^{\Sigma_k z(\alpha,k)}. \quad \text{(A5)}$$

The right-hand side is the desired quantity, i.e.,

$$\langle W_{i,\alpha,n} \rangle \to Q_i(N). \quad \text{(A6)}$$

Total number of times we repeated to obtain $\langle Q \rangle$, $N_s N_{\text{ext}}$, was between 30 000 and 50 000.

[1]See, for example, P. G. de Gennes, *Scaling Concepts in Polymer Physics* (Cornell University, Ithaca, 1979).

[2]T. Ohta and Y. Oono, Phys. Lett. A **89**, 460 (1982).

[3]T. Ohta and A. Nakanishi, J. Phys. A **16**, 4115 (1983).

[4]H. Okamoto, J. Chem. Phys. **83**, 2587 (1985).

[5]K. F. Freed, J. Chem. Phys. **79**, 15 (1983).

[6]For example, (a) B. Duplantier, J. Phys. (Paris) **43**, 991 (1982); (b) A. L. Kholodenko and K. F. Freed, J. Chem. Phys. **80**, 900 (1984).

[7]For example, (a) M. Daud, J. P. Cotton, B. Farnoux, G. Jannink, G. Sarma, B. Benoit, R. Duplessix, C. Picott, and P. G. de Gennes, Macromolecules **8**, 804 (1975); (b) I. Noda, Kato, T. Kitano, and M. Nagasawa, Macromolecules **14**, 668 (1981).

[8]K. Kremer, A. Baumgärtner, and K. Binder, Z. Phys. B **40**, 31 (1981).

[9]H. E. Stanley, P. J. Reynolds, S. Redner, and F. Family, *Real-Space Renormalization*, edited by T. W. Burkardt and J. M. van Leeuwen (Springer, New York, 1982), Chap. 7.

[10]F. T. Wall and F. Mandell, J. Chem. Phys. **63**, 4592 (1975).

[11]N. Metropolis, A. W. Rosenbluth, M. N. Rosenbluth, A. H. Teller, and E. Teller, J. Chem. Phys. **21**, 1087 (1953).

[12]The size effect had been studied by athermal 30-mer systems with different L's. When $L = 25$, for each of the systems of element site fractions $Nn/L^3 = 0.004$, 0.098, 0.200, 0.300, and 0.399, the values of $\langle S^2 \rangle$ were 9.58, 9.35, 8.95, 8.67, and 8.54, respectively. In this order, the values of $\ln\langle Q \rangle / L^3$ were 45.44, 43.87, 41.71, 38.95, and 35.50. When $L = 40$, for each of the systems of $Nn/L^3 = 0.0005$, 0.100, 0.200, 0.300, and 0.399, $\langle S^2 \rangle$ were 9.61, 9.25, 8.95, 8.67, and 8.45, respectively. In this order, $\ln\langle Q \rangle / L^3$ were 45.49, 43.88, 41.69, 38.96, and 35.45. [H. Okamoto, J. Chem. Phys. **79**, 3976 (1983).]

[13]H. Okamoto and A. Bellemans, J. Phys. Soc. Jpn. **47**, 955 (1979).

[14]S. K. Ma, *Modern Theory of Critical Phenomena* (Benjamin, London, 1976).

[15]I. D. Lawrie and S. Sarbach, *Phase Transitions and Critical Phenomena*, edited by C. Domb and J. L. Lebowitz (Academic, New York, 1984), Vol. 9, Chap. 1.

[16]H. E. Stanley, *Introduction to Phase Transitions and Critical Phenomena* (Clarendon, Oxford, 1971).

[17]M. Jannsens and A. Bellemans, Macromolecules **9**, 303 (1976).

[18]J. C. L. Guillou and J. Zinn-Justin, Phys. Rev. Lett. **39**, 95 (1977).

[19]P. Wiltzius, H. R. Haller, D. S. Cannell, and D. W. Schaefer, Phys. Rev. Lett. **51**, 1183 (1983).

[20]Y. Oono and K. F. Freed, J. Phys. A **15**, 1931 (1982).

[21]K. Kremer, A. Baumgärtner, and K. Binder, J. Phys. A **15**, 2879 (1981).

[22](a) B. Cherayil, J. F. Douglas, and K. F. Freed, J. Chem. Phys. **83**, 5293 (1985); (b) K. F. Freed, J. Phys. A **18**, 871 (1985).

[23]W. Bruns, Macromolecules **17**, 2825 (1984).